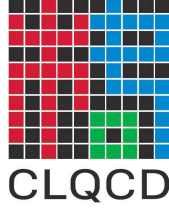


Low-energy DD scattering in lattice QCD



Pan-Pan Shi^{1,2,3,*} Feng-Kun Guo^{2,4,5,3,†} Chuan Liu^{6,7,8}
Liuming Liu^{9,4,‡} Peng Sun,^{9,4} Jia-Jun Wu^{4,3,§} and Hanyang Xing^{9,4}

¹*Instituto de Física Corpuscular (centro mixto CSIC-UV),
Institutos de Investigación de Paterna, Apartado 22085, 46071, Valencia, Spain*

²*CAS Key Laboratory of Theoretical Physics, Institute of Theoretical Physics,
Chinese Academy of Sciences, Beijing 100190, China*

³*Southern Center for Nuclear-Science Theory (SCNT), Institute of Modern Physics,
Chinese Academy of Sciences, Huizhou 516000, China*

⁴*School of Physical Sciences, University of Chinese Academy of Sciences, Beijing 100049, China*

⁵*Peng Huanwu Collaborative Center for Research and Education,
Beihang University, Beijing 100191, China*

⁶*School of Physics, Peking University, Beijing 100871, China*

⁷*Center for High Energy Physics, Peking University, Beijing 100871, China*

⁸*Collaborative Innovation Center of Quantum Matter, Beijing 100871, China*

⁹*Institute of Modern Physics, Chinese Academy of Sciences, Lanzhou, 730000, China*

We present the first lattice QCD calculation of single-channel DD scattering with quantum numbers $I(J^P) = 1(0^+)$ and $0(1^-)$. The calculation is performed on the 2 + 1 flavor Wilson-Clover ensembles with a lattice spacing $a \simeq 0.077$ fm and two different pion masses, $m_\pi \simeq 207$ and 305 MeV. The scattering parameters are determined using the Lüscher's finite volume method. Our results indicate weak repulsive interaction in the $1(0^+)$ channel and slightly attractive interaction in the $0(1^-)$ channel. The S -wave isovector DD scattering length and effective range, extrapolated to the physical pion mass, are (-0.26 ± 0.05) fm and (-5.5 ± 2.1) fm, respectively.

* Panpan.Shi@ific.uv.es

† fkguo@itp.ac.cn

‡ liuming@impcas.ac.cn

§ wujiajun@ucas.ac.cn

I. INTRODUCTION

Quantum Chromodynamics (QCD) is the fundamental theory that describes the strong interaction in terms of the quark and gluon degrees of freedom. However, in the low-energy region (at the energy scale close to Λ_{QCD}), a perturbative expansion in powers of the strong coupling constant fails, and thus alternative methods are required to study the strong interaction at this scale. One such method is lattice QCD (LQCD), which allows for investigations of the strong interaction in the nonperturbative regime from first principles. In LQCD, hadron scattering information can be extracted using Lüscher's finite-volume method [1–3] and its generalizations (for a review, see Ref. [4]). The method relates the energy spectrum of a two-particle system in the finite volume and the scattering information of the two particles in the continuum. Following this path, tremendous progress has been made with LQCD in understanding hadron spectra and interactions, see recent reviews in Refs. [4–7]. As for scatterings of identical spinless mesons, $\pi\pi$ scattering has been extensively investigated by several LQCD groups for various isospin channels $I = 0, 1$ and 2 [8–16], and KK scattering in the $I = 1$ channel has also been explored in Refs. [15–18]. Here we will focus on DD scattering in the low-energy regime.

DD scattering is related to the study of exotic states in the doubly charmed sector. In particular, the doubly charmed exotic meson $T_{cc}(3875)^+$, which couples strongly to the isoscalar DD^* in the S wave, was observed in the $D^0 D^0 \pi^+$ invariant mass distribution by LHCb [19, 20]. Information on DD scattering can provide insights into the DD final state interactions that influences predictions on the T_{cc}^+ width [21–23].¹ Actually, the phenomenological calculation in Ref. [21] displayed a sizeable impact of the DD final state interaction on the T_{cc} width based on the one-Boson-exchange model [26]. In addition, the DDK three-body bound state has been predicted in both continuum [27–30] and finite volume formalisms [31, 32]. So far, in the inclusive decay processes of $\Upsilon(1S)$ and $\Upsilon(2S)$ [33], the Belle Collaboration has not found significant signals associated with this state in the $D^+ D_s^{*+}$ invariant mass distribution. To further investigate the possible DDK bound state, model-independent input on DD two-body scattering is essential.

LQCD has been employed to study the interaction of the DD^* system. The DD^* scattering [34–36] and the $DD^*-D^*D^*$ coupled-channel scattering [37] have been explored using the interpolating operators of DD^* and both DD^* and D^*D^* , respectively. Additionally, the quark mass dependence of T_{cc}^+ has been analyzed with DD^* and D^*D^* interpolating operators [38] (see also Ref. [39]). While analyzing the LQCD data for the DD^* system, it was noted that the one-pion exchange long-range

¹ For explorations on the influence of the analogous $D\bar{D}$ final state interaction on the open-charm decay width for $X(3872) \rightarrow D^0 \bar{D}^0 \pi$, see Refs. [24, 25].

force (the associated left-hand cut and a zero of the scattering amplitude) could significantly affect the extraction of scattering information [40]. Several approaches have been proposed to address this issue [41–45]. One natural solution is to include the $DD\pi$ three-body operator in the DD^* scattering process. However, the lack of isovector DD and isoscalar $DD\pi$ scattering information hinders further precise studies of the T_{cc}^+ [44].

This work presents the first LQCD calculation of DD scattering based on the $2 + 1$ flavor full QCD ensembles. The Lüscher finite volume method is utilized to connect the finite-volume energy levels to infinite-volume scattering parameters. We compute the energy levels with the DD interpolating operators for both $I = 1$ and $I = 0$. The scattering length and effective range for both S - and P -wave channels are extracted. The calculations are performed at two different pion masses, $m_\pi \simeq 305$ MeV and $m_\pi \simeq 207$ MeV. The pion mass dependence of the S -wave scattering length and effective range is explored.

This paper is organized as follows. In Sect. II, details of the lattice setup and methodology are introduced. In Sect. III, we discuss the single- and two-meson operators as well as the method for the extraction of the energy levels from correlation functions. The formula, involving the Lüscher equation modified by the dispersion relation and the parameterization of phase shift, is discussed in Sect. IV. The S - and P -wave scattering information for the isovector and isoscalar DD channels, including the scattering lengths, effective ranges, and the phase shifts, are present in Sect. V. We explore the pion mass dependence of the S -wave scattering length and effective range in Sect. VI. A conclusion is given in Sect. VII. Finally, Appendix A contains details of derivation of Lüscher equation with the modified dispersion relation.

II. LATTICE SETUP

The results presented in this paper are based on the gauge configurations generated by the CLQCD Collaboration with $2 + 1$ dynamical quark flavors using the tadpole improved tree-level Symanzik gauge action and Clover fermion action [46]. Numerous studies have been performed on these configurations, see, e.g., Refs. [47–53]. In this work, we use four ensembles with the same lattice spacing $a = 0.07746$ fm and two different pion masses $m_\pi \simeq 305$ MeV and $m_\pi \simeq 207$ MeV. Details of the ensembles are listed in Table I. Among these ensembles, F32P21/F48P21 and F32P30/F48P30 are two couples that share the same pion mass but have different volumes to obtain more kinematic points in the finite-volume spectra, rendering a more stable and precise determination of the scattering parameters. The valence charm quark action is the same as the

TABLE I. Parameters of the ensembles, including the name, the lattice spacing a , the pion mass m_π , the volume size $L^3 \times T$, and the number of configurations N_{conf} .

Ensembles	a [fm]	m_π [MeV]	$(L/a)^3 \times T/a$	N_{conf}
F32P30	0.07746(18)	305.2(13)	$32^3 \times 96$	371
F48P30	0.07746(18)	305.4(9)	$48^3 \times 96$	201
F32P21	0.07746(18)	207.9(22)	$32^3 \times 64$	201
F48P21	0.07746(18)	207.2(11)	$48^3 \times 96$	223

light/strange quark action used in the ensembles, and the charm quark mass is tuned to reproduce the spin-averaged $1S$ -charmonium mass, $m_{\text{av}} = (m_{\eta_c} + 3m_{J/\psi})/4$.

The quark propagators are computed with the distillation quark smearing method [54], which improves the precision and allows for the inclusion of many interpolating operators in the calculation of the correlation functions. The smearing operator is composed of a small number (N_{ev}) of the eigenvectors associated with the N_{ev} lowest eigenvalues of the three-dimensional Laplacian defined in terms of the HYP(hypercubic)-smeared gauge field. The number of eigenvectors N_{ev} is 100 for all four ensembles. We also tried $N_{\text{ev}}=200$ for the ensembles F48P21 and F48P30, and the obtained energies were consistent with those with $N_{\text{ev}}=100$. The statistical uncertainty is estimated by the bootstrap method with 4000 bootstrap samples.

III. CALCULATION OF THE ENERGY LEVELS

In LQCD, the finite-volume spectra are extracted from the two-point correlation functions

$$\mathcal{C}_{ij}(t) = \sum_{t_s} \left\langle \mathcal{O}_i(t + t_s) \mathcal{O}_j^\dagger(t_s) \right\rangle, \quad (1)$$

where \mathcal{O}_i and \mathcal{O}_j are the interpolating operators carrying the quantum numbers of the system of interest. The source time t_s spans all time slices to increase statistics.

The single D -meson operators are $\mathcal{O}_{D^+}(\mathbf{x}, t) = \bar{d}\gamma_5 c(\mathbf{x}, t)$ and $\mathcal{O}_{D^0}(\mathbf{x}, t) = \bar{u}\gamma_5 c(\mathbf{x}, t)$ for the charged and neutral D , respectively. The momentum projected operator is defined as $\mathcal{O}(\mathbf{p}, t) = \sum_{\mathbf{x}} e^{-i\mathbf{p}\cdot\mathbf{x}} \mathcal{O}(\mathbf{x}, t)$. The dispersion relation of the D meson $E^2 = m_D^2 + Zp^2$, with $p \equiv \sqrt{\mathbf{p}^2}$, is investigated by calculating the single-particle energy at the five lowest momenta on lattice: $\mathbf{p} = (0, 0, 0)$, $(0, 0, 1)$, $(0, 1, 1)$, $(1, 1, 1)$ and $(0, 0, 2)$ (in units of $2\pi/L$). The parameters m_D and Z , listed

TABLE II. Parameters for the dispersion relation of the D meson.

	F32P30	F48P30	F32P21	F48P21
m_D [MeV]	1966.6(8)	1966.0(6)	1903.9(16)	1900.3(5)
Z	0.926(7)	0.946(9)	0.941(1)	0.976(6)

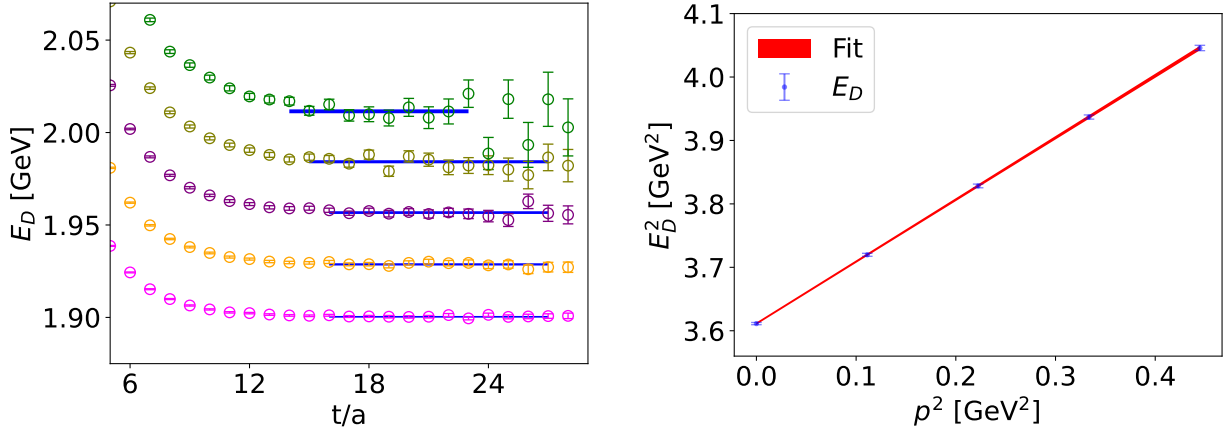


FIG. 1. Effective energies and the dispersion relation of the D meson for the ensemble F48P21. The left panel presents five energies of the D meson at the five lowest momenta, and the right panel presents a fit to the dispersion relation to these energies.

in Table II, are determined by fitting the five energies to the dispersion relation. As an example, the five energies and the dispersion relation for the ensemble F48P21 are shown in Fig. 1. In the continuum limit, Z should be unity. However, due to lattice artifacts, it may take a different value. The original Lüscher's formula assumes the continuum dispersion relation. In order to account for the effects of the deviation from the continuum dispersion relation, we modify the Lüscher's formula as elaborated in Appendix A.

The interacting energy levels of two particles are extracted from the correlation functions of the two-particle operators. The interpolating operators for the isovector and isoscalar DD systems are given by

$$\mathcal{O}_{DD,I=1}^{\mathbf{P},\Lambda,\mu} = \frac{1}{\sqrt{2}} \sum_{\mathbf{p}_1, \mathbf{p}_2} \mathcal{C}(\mathbf{P}, \Lambda, \mu, \mathbf{p}_1, \mathbf{p}_2) (\mathcal{O}_{D^+}(\mathbf{p}_1) \mathcal{O}_{D^0}(\mathbf{p}_2) + \mathcal{O}_{D^0}(\mathbf{p}_1) \mathcal{O}_{D^+}(\mathbf{p}_2)), \quad (2)$$

$$\mathcal{O}_{DD,I=0}^{\mathbf{P},\Lambda,\mu} = \frac{1}{\sqrt{2}} \sum_{\mathbf{p}_1, \mathbf{p}_2} \mathcal{C}(\mathbf{P}, \Lambda, \mu, \mathbf{p}_1, \mathbf{p}_2) (-\mathcal{O}_{D^+}(\mathbf{p}_1) \mathcal{O}_{D^0}(\mathbf{p}_2) + \mathcal{O}_{D^0}(\mathbf{p}_1) \mathcal{O}_{D^+}(\mathbf{p}_2)), \quad (3)$$

where $\mathbf{P} = \mathbf{p}_1 + \mathbf{p}_2$ is the total momentum, Λ denotes the irreducible representation (irrep) of the octahedral group and its subgroups, which are the spatial rotational symmetry groups on lattice,

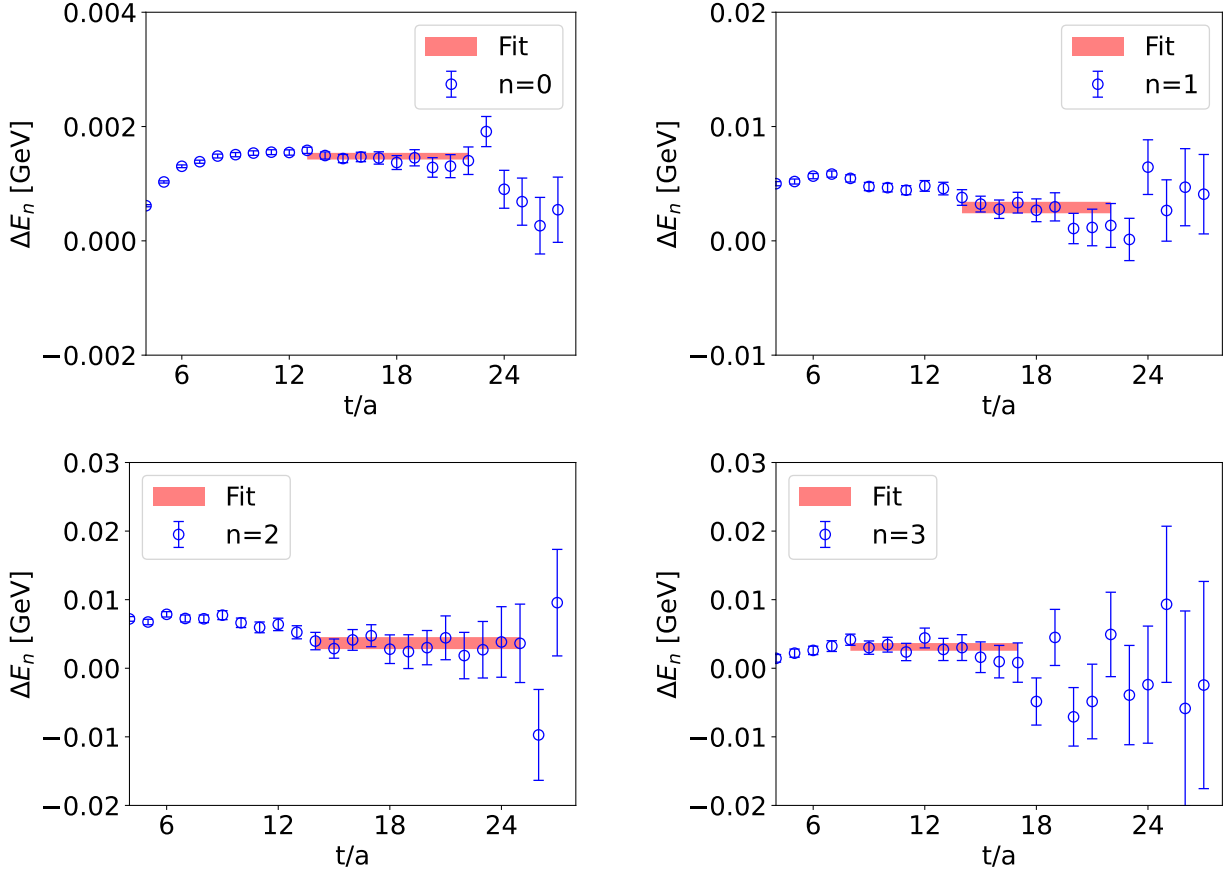


FIG. 2. Effective energy splittings $\Delta E_n = \log R_n(t+1)/R_n(t)$ for the A_1^+ irrep on the ensemble F48P21. The red horizontal bars indicate the fitted ΔE_n and the fit ranges.

μ denotes the irrep row, and $\mathcal{C}(\mathbf{P}, \Lambda, \mathbf{p}_1, \mathbf{p}_2)$'s are the Clebsch-Gordan coefficients. In this work, we only compute the energies in the rest frame ($\mathbf{P} = \mathbf{0}$) and the momenta of the single particles up to $|\mathbf{p}_1| = |\mathbf{p}_2| = 2$. For $I = 1$, the operators reside in the A_1^+ , E^+ and T_2^+ irreps, while for $I = 0$, the operators are in the T_1^- , T_2^- , and A_2^- irreps. The relevant Clebsch-Gordan coefficients are provided in Appendix A of Ref. [11].

After computing the correlation functions, we employ the generalized eigenvalue problem (GEVP) method [55] to determine the energy levels in each irrep. The GEVP is solved as follows:

$$\mathcal{C}(t)v_n(t, t_0) = \lambda_n(t, t_0)\mathcal{C}(t_0)v_n(t, t_0). \quad (4)$$

Here, t_0 is set to 2, and we have checked that different choices of t_0 did not lead to noticeable impact on the determination of the energy levels. The energy levels are extracted from the ratio

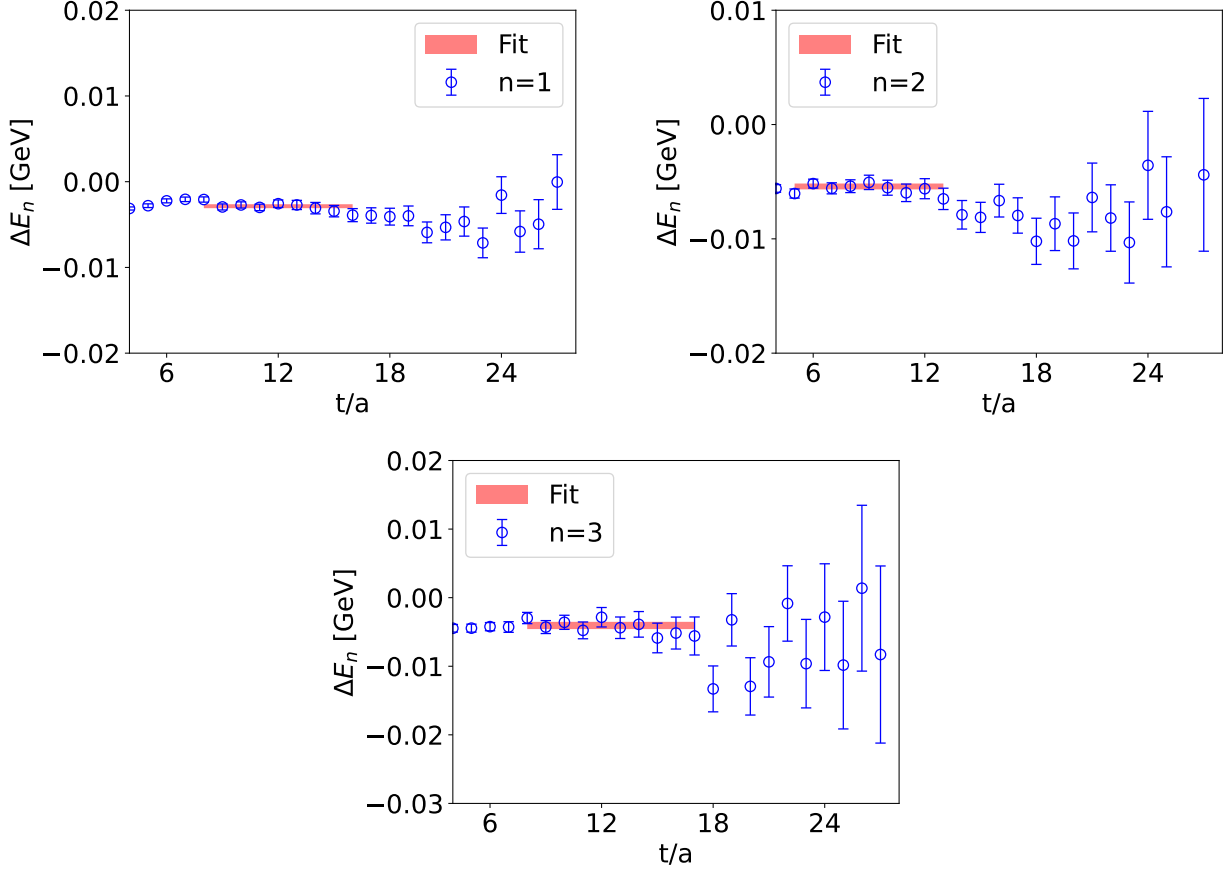


FIG. 3. Same as Fig. 2 but for the T_1^- irrep.

of the eigenvalues $\lambda_n(t)$ to the single-particle correlation functions

$$R_n(t) = \frac{\lambda_n(t)}{\mathcal{C}_D^{\mathbf{p}_n}(t)\mathcal{C}_D^{\mathbf{p}_n}(t)} = A'e^{-\Delta E_n t}, \quad (5)$$

where $\mathcal{C}_D^{\mathbf{p}_n}(t)$ is the single D correlation function with momentum \mathbf{p}_n , ΔE_n is the splitting between the energies of the interacting DD system and two free D mesons. In the DD system, where the interacting energy levels are quite close to the free energy levels, this method can partially cancel correlated statistical fluctuations and reduce the contributions of excited states by fitting the ratio $R_n(t)$, and therefore help us distinguish energy levels that nearly degenerate with the free ones. The effective energies of the lowest four and three energy splittings ΔE_n for A_1^+ and T_1^- irreps on the F48P21 ensemble, are shown in Figs. 2 and 3, respectively. The interacting energies are then obtained by $E_n = \Delta E_n + E_n^{\text{free}}$ with E_n^{free} the free energy levels.

The obtained energy levels for all irreps are presented in Figs. 4 and 5. The results show that, in the A_1^+ irreps, the lowest energy level for each pion mass is slightly above the DD threshold (see also Fig. 2), indicating a weak repulsive interaction in the S -wave $I = 1$ DD system. The energy

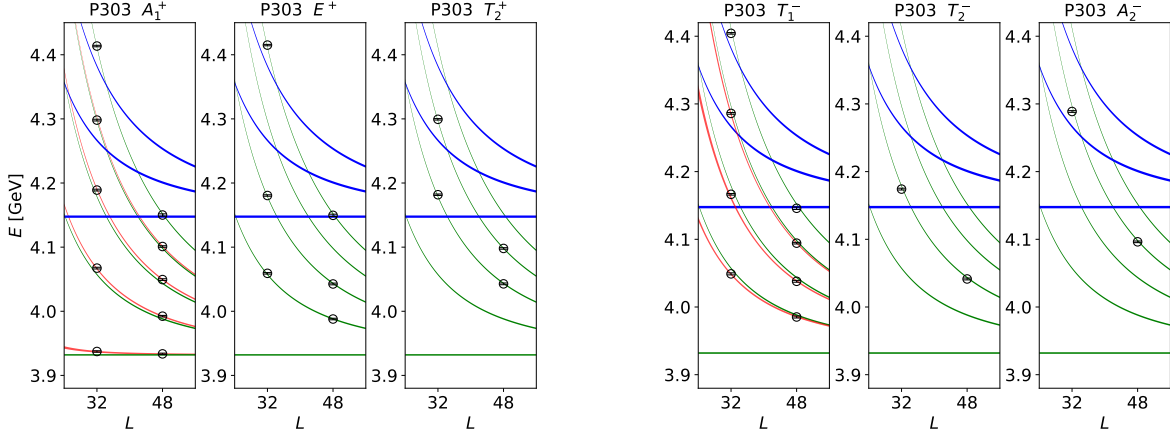


FIG. 4. Energy levels for the DD system with a pion mass $m_\pi \simeq 305$ MeV. The green and blue bands represent the free energy levels for DD and D^*D^* systems, respectively. These free energy levels are calculated using the continuum dispersion relation (i.e., $Z = 1$) with the parameters from the ensembles with lattice size $L = 48$. For the $L = 32$ lattice, the interacting energy levels are shifted based on the gap between the free energy levels in different finite volumes. The red bands denote the interacting energy levels fitted by the ERE parameterization. The width of the bands reflects the statistical uncertainty.

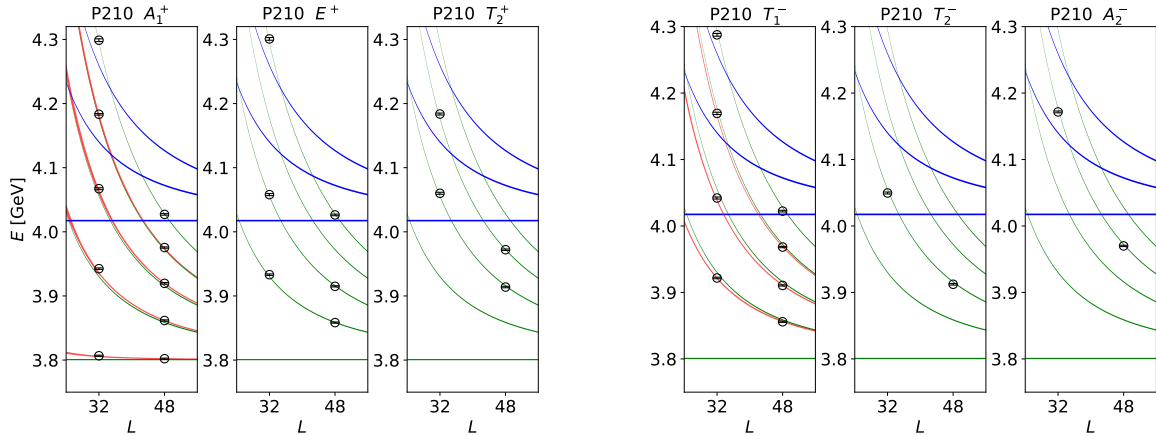


FIG. 5. Energy levels for the DD system with pion mass $m_\pi \simeq 207$ MeV for the case $Z = 1$. The colour bands are the same as that in Fig. 4.

levels in the E^+ and T_2^+ irreps almost coincide with the free ones within the current statistical precision, indicating negligible interactions in the D -wave and higher partial waves (the angular momenta of different irreps are listed in Table III). In the following, we will ignore the mixing from higher partial waves and utilize the energy levels below the D^*D^* threshold, to avoid possible contamination from D^*D^* , in the A_1^+ irrep to determine the S -wave DD scattering parameters in the $I = 1$ channel. Based on similar observations in the T_1^- , T_2^- , and A_2^- irreps, we use the energy

TABLE III. Irreps and the relative quantum numbers (orbital angular momentum L and parity P) for the $I = 1$ DD with $L \leq 4$ partial waves in the rest frame.

Λ^P	A_1^+	A_2^-	E^+	T_1^-	T_2^+	T_2^-
L	0, 4	3	2, 4	1, 3	2, 4	3

levels in the T_1^- irrep to determine the P -wave DD scattering parameters in the $I = 0$ channel.

IV. FORMALISM AND FITTING STRATEGY

For two-meson scattering, the partial-wave phase shift δ_l is obtained from the determinant of the Lüscher matrix,

$$\det (M_{lm,l'm'}(\tilde{p}) - \delta_{ll'}\delta_{mm'}\cot \delta_l) = 0, \quad (6)$$

where $\tilde{p} = pL/(2\pi)$ is related to the on-shell momentum p . The energy levels are calculated within the specific little group. By selecting a particular basis for the irrep Λ , the determinant, according to Schur's lemma, reduces to [3, 14, 56]

$$\det (M_{ln,l'n'}^\Lambda(\tilde{p}) - \delta_{ll'}\delta_{nn'}\cot \delta_l) = 0, \quad (7)$$

where $n(n')$ denotes the order of the irrep Λ . To further simplify the Lüscher matrix in a specific irrep, we define the function

$$\omega_{js}(\tilde{p}) = \frac{1}{\pi^{3/2}\sqrt{2j+1}} \frac{\omega_1(p) + \omega_2(p)}{Z_1\omega_2(p) + Z_2\omega_1(p)} \frac{\mathcal{Z}_{js}(\tilde{p})}{\tilde{p}^{j+1}}, \quad (8)$$

where $\omega_{1,2}(p) \equiv \sqrt{m_{1,2}^2 + Z_{1,2}p^2}$, \mathcal{Z}_{js} is the zeta function. Compared to the original Lüscher formula, there is an extra factor $[\omega_1(p) + \omega_2(p)]/[Z_1\omega_2(p) + Z_2\omega_1(p)]$, accounting for the deviation of the dispersion relation from the continuum one. We refer to Appendix A for detailed discussion.

In this work, we focus on extracting the partial-wave phase shifts for $L = 0$ and $L = 1$, while the high partial-wave contributions are neglected. For the A_1^+ and T_1^- irreps, the determinants of Eq. (7) are reduced to

$$-\cot \delta_0 + \omega_{00}(\tilde{p}_A) = 0, \quad -\cot \delta_1 + \omega_{00}(\tilde{p}_T) = 0, \quad (9)$$

where the coefficients of $\omega_{js}(\tilde{p})$ are taken from Ref. [3], and the subscripts A and T denote the momenta for the A_1^+ and T_1^- irreps, respectively.

Instead of translating the phase shift from interacting energy levels via Eq. (9), we parameterize the phase shift using the effective range expansion (ERE) and constrain the relevant parameters by fitting the energy levels in different irreps. The ERE reads

$$\cot \delta_l = p^{-2l-1} \left(\frac{1}{a_l} + \frac{1}{2} r_l p^2 + \mathcal{O}(p^4) \right), \quad (10)$$

where a_l and r_l are the scattering length and effective range for the l -wave, respectively. Two scenarios are considered to determine a_l and r_l : $Z \neq 1$, where Z is fixed to the values given in Table II, and $Z = 1$. In each case, the interacting energy levels are calculated using the formula $E_n = \Delta E_n + 2\sqrt{m_D^2 + Z\mathbf{q}_n^2}$. To minimize possible coupled-channel effects from D^*D^* , we only use the first two energy levels and four energy levels for the ensembles F32P30 and F48P30 to fit the S -wave scattering length a_0 and effective range r_0 in the A_1^+ irrep. For the T_1^- irrep, the first one and three energy levels for the ensemble F32P30 and F48P30 are employed to get the corresponding P -wave ERE parameters, respectively. In addition, for the ensemble F48P21, the first three energy levels in the A_1^+ and T_1^- irreps are used to determine the S - and P -waves ERE parameters, respectively. The energy levels for the ensemble F32P21 are neglected due to the small finite volume.

V. SCATTERING ANALYSIS RESULTS

The S - and P -wave ERE parameters are shown in Table IV. In the case of S -wave scattering, both the scattering length a_0 and effective range r_0 are negative. In contrast, a_1 and r_1 for the P -wave are positive. Notably, the absolute value of a_0 is about one order-of-magnitude smaller than r_0 . The situation, where $|a_0| \ll |r_0|$, also occurs in the $I = 2 \pi\pi$ and $I = 1 KK$ systems, as found in Refs. [10, 16]. Near the free energy levels, the Lüscher's zeta function becomes highly sensitive to small variations of energy levels. Compared to the lowest interacting energy levels in A_1^+ irrep, the statistical uncertainties of other energy levels are enlarged by this sensitivity. Consequently, the parameters r_0 , a_1 and r_1 have large statistical uncertainties.

As listed in Table IV, differences of the ERE parameters between the $Z \neq 1$ and $Z = 1$ cases are within 1σ . However, the $Z = 1$ case exhibits smaller statistical uncertainties in the ERE parameters as the Z values in Table II bare uncertainties.

The phase shifts for the $I(J^P) = 1(0^+)$ and $0(1^-)$ DD scattering calculated using $Z = 1$ are shown in Fig. 6. In our convention, as the energy E increases, the S -wave phase shift δ_0 decreases, while the P -wave phase shift δ_1 increases. Since there is no bound-state energy level below the

TABLE IV. ERE parameters for the S - and P -wave DD scattering. The χ^2 value per degrees of freedom (d.o.f.) for the fits are also given. The cases for $Z \neq 1$ and $Z = 1$ denote that the discrete and continuum dispersion relations are used to determine a_l and r_l , respectively.

	F32P30/F48P30 ($m_\pi = 305$ MeV)		F32P21/F48P21 ($m_\pi = 207$ MeV)	
	$Z \neq 1$	$Z = 1$	$Z \neq 1$	$Z = 1$
a_0 [fm]	-0.23(3)	-0.24(3)	-0.23(6)	-0.25(3)
r_0 [fm]	-1.67(24)	-1.81(21)	-4.1(31)	-4.3(14)
$\chi^2/\text{d.o.f.}$	0.55	1.22	0.96	0.96
a_1 [fm ³]	2.1(22)	1.7(21)	1.2(18)	0.9(17)
r_1 [fm ⁻¹]	17.4(55)	16.8(52)	20.4(38)	18.6(38)
$\chi^2/\text{d.o.f.}$	0.63	0.68	0.78	1.08

threshold, the opposite signs for δ_0 and δ_1 indicate repulsive and attractive interactions for the S - and P -wave DD systems, respectively.

VI. PION MASS DEPENDENCE

Our results are obtained at two unphysically large pion masses. In order to determine the scattering length and effective range at the physical pion mass, we parameterize the a_0 and r_0 as functions of the pion mass and investigate their pion mass dependence for the continuum dispersion relation (the $Z = 1$ case). We do not perform the extrapolation for the P -wave ERE parameters due to the large statistical uncertainties associated with them.

Since there are only two different pion masses, we parametrize the scattering length and effective range as simple polynomial functions:

$$a_0(m_\pi) = c_0^a + c_1^a m_\pi^2, \quad r_0(m_\pi) = c_0^r + c_1^r m_\pi^2, \quad (11)$$

where the parameters c_0^a , c_1^a , c_0^r , and c_1^r can be determined using the results in Table IV, corresponding to pion masses $m_\pi \approx 207$ and 305 MeV for the ensembles F32P21/F48P21 and F32P30/F48P30, respectively. The parameters are found to be $c_0^a = -0.26(6)$ fm, $c_1^a = 0.010(33)$ fm³, $c_0^r = -6.4(27)$ fm, and $c_1^r = 1.9(11)$ fm³. With the extrapolation formulae in Eq. (11), the S -wave isovector DD

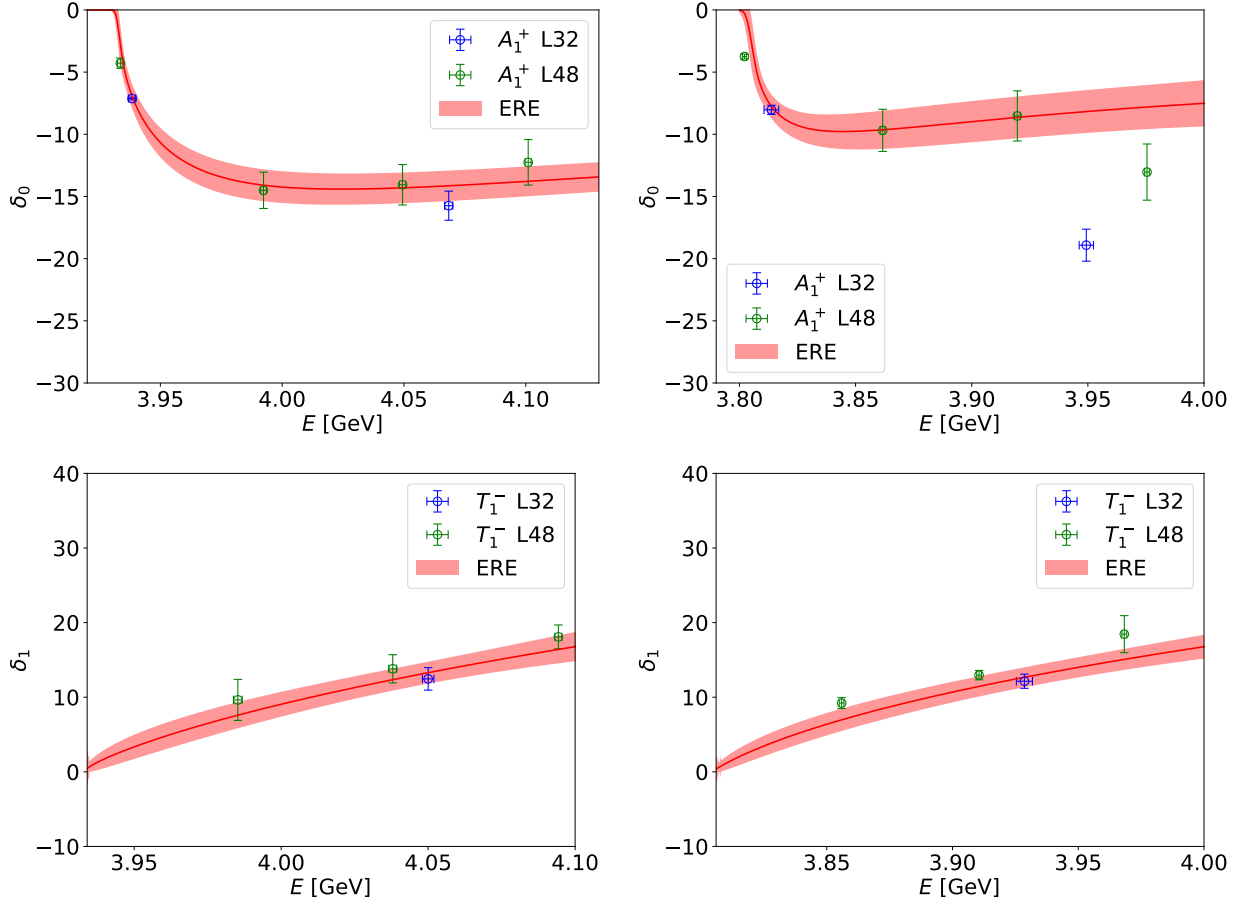


FIG. 6. S - (the first row) and P -wave (the second row) DD scattering phase shifts for $Z = 1$ case. The left and right panels are the results for $m_\pi \approx 305$ MeV and 207 MeV, respectively. The red lines denote the phase shifts calculated from the best fit ERE parametrization and the bands represent the statistical uncertainty.

scattering length and effective range at the physics pion mass are predicted to be

$$a_0^{\text{phy}} = -0.26(5) \text{ fm}, \quad r_0^{\text{phy}} = -5.5(21) \text{ fm}, \quad (12)$$

and the values at the chiral limit are

$$a_0^\chi = -0.26(6) \text{ fm}, \quad r_0^\chi = -6.4(27) \text{ fm}, \quad (13)$$

where the uncertainties are purely statistical.

The pion mass dependence of scattering length and effective range is displayed in Fig. 7. A more robust chiral extrapolation to the physical pion mass requires results at more pion masses in a broader range. Since we only have one lattice spacing, we are unable to extrapolate our results to the continuum limit.

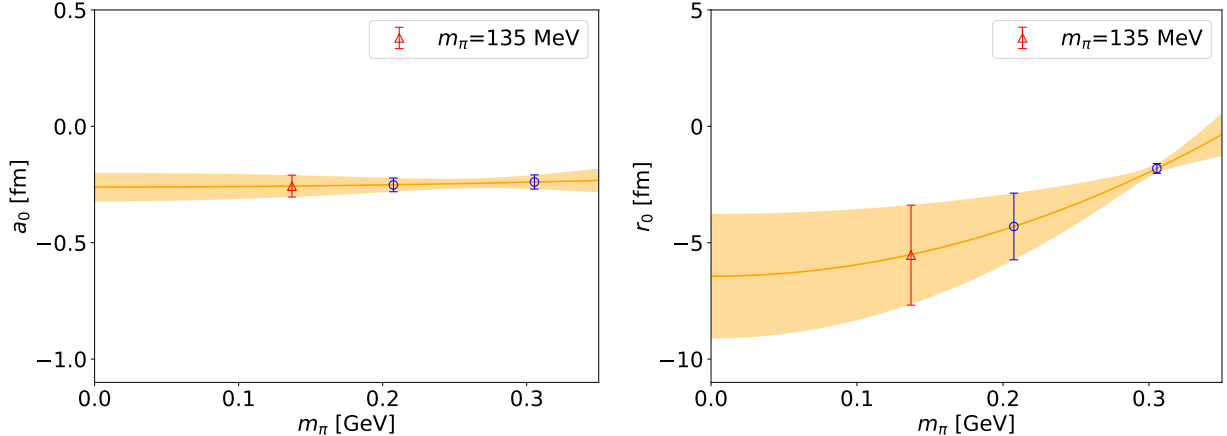


FIG. 7. Extrapolation of S -wave scattering length a_0 and effective range r_0 for $Z = 1$ case. The blue bars are extracted from energy levels in A_1^+ irrep, and the red bars indicate the physical results.

VII. CONCLUSIONS

Utilizing the 2+1 flavor full QCD Wilson-Clover configurations, we calculated the DD scattering in the $I(J^P) = 1(0^+)$ and $0(1^-)$ channels at two different pion masses 207 and 350 MeV. Due to the lattice artifacts, the dispersion relation of D meson on lattice deviates from the continuum dispersion relation. We modified the original Lüscher formula to incorporate this deviation. The S - and P -wave ERE parameters were extracted from the interacting energy levels, and the chiral extrapolation to the physical pion mass was performed. Our results indicate a weak repulsive interaction in the $I(J^P) = 1(0^+)$ DD scattering channel and a slight attractive interaction in the $I(J^P) = 0(1^+)$ channel. From a phenomenological point of view, the S -wave isovector $D^{(*)}D^{(*)}$ interactions from exchanging the light vector mesons ρ and ω are repulsive while the isoscalar ones are attractive [57], and recent lattice studies indeed indicate the importance of the t -channel light vector-meson exchange in the DD^* scattering [35, 58].

In this initial investigation, we focus on single-channel DD scattering in the energy range below the D^*D^* threshold. In future studies, the DD - D^*D^* coupled-channel scattering will be considered. Furthermore, lattice data with a broader range of pion masses and various lattice spacings are required to control the systematic uncertainties in a more robust way.

ACKNOWLEDGMENTS

We are grateful to Yi-Qi Geng for useful discussions. We thank the CLQCD collaborations for providing us the gauge configurations [46], which are generated on the HPC Cluster of ITP-CAS, the Southern Nuclear Science Computing Center (SNSC), the Siyuan-1 cluster supported by the Center for High Performance Computing at Shanghai Jiao Tong University and the Dongjiang Yuan Intelligent Computing Center. Softwares **Chroma** [59] and **QUDA** [60–62] were used to generate the configurations and solve the perambulators. This work is partially supported by the National Key R&D Program of China under Grant No. 2023YFA1606703; by the Chinese Academy of Sciences (CAS) with Grants No. XDB34030000 and No. YSBR-101; by the Generalitat Valenciana (GVA) for the project with ref. CIDEAGENT/2019/015; by the Spanish Ministerio de Ciencia e Innovación (MICINN) under contract PID2020-112777GB-I00; by the National Natural Science Foundation of China (NSFC) under Grants No. 12293060, No. 12293061, No. 12175279, No. 12125507, No. 12361141819, No. 12047503, No. 12221005 and No. 12175239; and by Guangdong Major Project of Basic and Applied Basic Research under Grant No. 2020B0301030008.

Appendix A: Effect of the dispersion relation to Lüscher Equation

The Lüscher’s finite volume method [1–3] enables us to extract the scattering information from the finite-volume spectra which can be calculated in lattice QCD. The original Lüscher’s formula are derived by assuming the continuum dispersion relation. However, on lattice, the continuum dispersion relation is usually broken due to lattice artifacts, especially for the heavy-flavor hadrons. To incorporate the effect of the discrete dispersion relation into the Lüscher quantization condition, we start from the partial-wave Lippmann-Schwinger equation in the finite volume. The energy levels are given by poles of partial-wave T -matrix in the finite volume with a specific lattice size L [2, 63–66]. The finite-volume partial-wave T -matrix with the angular momentum l (l') and its third component m (m') for initial (final) states is

$$\tilde{T}_{lm,l'm'}(p) = V_l(p)\delta_{ll'}\delta_{mm'} + \sum_{l''m''} V_l(p)\tilde{G}_{lm,l''m''}(p)\tilde{T}_{l''m'',l'm'}(p), \quad (\text{A1})$$

where $V_l(p)$ is the short-distance potential and p is the on-shell momentum. In the finite volume, the Green’s function $\tilde{G}_{lm,l'm'}$ is

$$\tilde{G}_{lm,l'm'}(p) = \frac{4\pi}{L^3} \sum_{\mathbf{q}_n}^{|\mathbf{q}_n| < \Lambda} \left(\frac{|\mathbf{q}_n|}{p}\right)^{l+l'} Y_{lm}^*(\hat{\mathbf{q}}_n) I(\mathbf{q}_n) Y_{l'm'}(\hat{\mathbf{q}}_n), \quad (\text{A2})$$

with a cutoff Λ and $\hat{\mathbf{q}}_n = \mathbf{q}_n/|\mathbf{q}_n|$. Considering the dispersion relation $\omega_i(\mathbf{q}) = \sqrt{m_i^2 + Z_i \mathbf{q}^2}$ and $\sqrt{s} = \omega_1(p) + \omega_2(p)$ in the center-of-mass frame, the function $I(\mathbf{q}_n)$ is expressed as

$$I(\mathbf{q}) = \frac{1}{4\omega_1(\mathbf{q})\omega_2(\mathbf{q})} \frac{1}{\sqrt{s} - (\omega_1(\mathbf{q}) + \omega_2(\mathbf{q}))} \approx \frac{1}{2[Z_1\omega_2(p) + Z_2\omega_1(p)]} \frac{1}{p^2 - \mathbf{q}^2}, \quad (\text{A3})$$

by just keeping the positive-energy pole contribution using

$$\begin{aligned} & \lim_{|\mathbf{q}| \rightarrow p} \frac{1}{4\omega_1(\mathbf{q})\omega_2(\mathbf{q})} \frac{p^2 - \mathbf{q}^2}{\sqrt{s} - \omega_1(\mathbf{q}) - \omega_2(\mathbf{q})} \\ &= \lim_{|\mathbf{q}| \rightarrow p} \frac{1}{4\omega_1(\mathbf{q})\omega_2(\mathbf{q})} \frac{2p}{\frac{Z_1 p}{\omega_1(p)} + \frac{Z_2 p}{\omega_2(p)}} = \lim_{|\mathbf{q}| \rightarrow p} \frac{1}{2[Z_1\omega_2(p) + Z_2\omega_1(p)]}. \end{aligned} \quad (\text{A4})$$

Using the identity for standard spherical harmonics $Y_{lm}(\hat{\mathbf{q}})$,

$$Y_{lm}^*(\hat{\mathbf{q}})Y_{l'm'}(\hat{\mathbf{q}}) = \sum_{js} (-1)^{m'} \sqrt{\frac{(2l+1)(2j+1)(2l'+1)}{4\pi}} Y_{js}(\hat{\mathbf{q}}) \begin{pmatrix} l & j & l' \\ m & s & m' \end{pmatrix} \begin{pmatrix} l & j & l' \\ 0 & 0 & 0 \end{pmatrix}, \quad (\text{A5})$$

the finite-volume Green's function in Eq. (A2) can be reduced to

$$\tilde{G}_{lm,l'm'}(p) = \frac{4\pi}{L^3} \sum_{\mathbf{q}_n}^{|\mathbf{q}_n| < \Lambda} \sum_{j,s} \left(\frac{|\mathbf{q}_n|}{p} \right)^{l+l'-j} \frac{1}{\sqrt{4\pi}} C_{lm,js,l'm'} \left(\frac{|\mathbf{q}_n|}{p} \right)^j Y_{js}(\hat{\mathbf{q}}_n) I(\mathbf{q}_n), \quad (\text{A6})$$

where $C_{lm,js,l'm'}$ are the Clebsch-Gordan coefficients given by

$$C_{lm,js,l'm'} = (-1)^{m'} \sqrt{(2l+1)(2j+1)(2l'+1)} \begin{pmatrix} l & j & l' \\ m & s & m' \end{pmatrix} \begin{pmatrix} l & j & l' \\ 0 & 0 & 0 \end{pmatrix}. \quad (\text{A7})$$

Here the factor $(|\mathbf{q}_n|/p)^{l+l'-j}$ can be replaced by unity, while $(|\mathbf{q}_n|/p)^j$ is necessary so that the subtraction does not introduce a singularity at $\mathbf{q} = 0$ for $Y_{js}(\hat{\mathbf{q}})$ [65, 66].

For the single channel, the l -wave T -matrix in the infinite volume is parameterized as

$$T_l(p) = \frac{8\pi\sqrt{s}}{p \cot \delta_l - ip}. \quad (\text{A8})$$

The finite-volume T -matrix element then is

$$\begin{aligned} \tilde{T}_{lm,l'm'}^{-1}(p) &= T_{lm,l'm'}^{-1} - \left[\tilde{G}_{lm,l'm'}(p) - \int^{|\mathbf{q}| < \Lambda} \frac{d^3\mathbf{q}}{(2\pi)^3} I(\mathbf{q}) 4\pi Y_{lm}^*(\hat{\mathbf{q}}) Y_{l'm'}(\hat{\mathbf{q}}) \right] \\ &= \frac{p}{8\pi\sqrt{s}} [\delta_{ll'} \delta_{mm'} \cot \delta_l - \mathcal{M}_{lm,l'm'}(p)], \end{aligned} \quad (\text{A9})$$

where the matrix $\mathcal{M}_{lm,l'm'}$ can be expressed as the Lüscher zeta function as follows,

$$\mathcal{M}_{lm,l'm'}(p) \equiv \frac{1}{\pi^{3/2}} \frac{\omega_1(p) + \omega_2(p)}{Z_1\omega_2(p) + Z_2\omega_1(p)} \sum_{j,s} \left(\frac{2\pi}{Lp} \right)^{j+1} \mathcal{Z}_{js} \left(\left(\frac{Lp}{2\pi} \right)^2 \right) C_{lm,js,l'm'}. \quad (\text{A10})$$

Here $\mathcal{Z}_{js}(q^2)$ is the Lüscher's zeta function in the rest frame,

$$\mathcal{Z}_{js}(q^2) = \sum_{\mathbf{n} \in \mathbb{Z}^3} \frac{\mathbf{n}^j Y_{js}(\hat{\mathbf{n}})}{\mathbf{n}^2 - q^2}. \quad (\text{A11})$$

The energy levels finally are associated with the infinite-volume phase shift

$$\det [\cot \delta - \mathcal{M}(p)] = 0. \quad (\text{A12})$$

-
- [1] M. Lüscher, *Commun. Math. Phys.* **104**, 177 (1986).
[2] M. Lüscher, *Commun. Math. Phys.* **105**, 153 (1986).
[3] M. Lüscher, *Nucl. Phys. B* **354**, 531 (1991).
[4] R. A. Briceño, J. J. Dudek, and R. D. Young, *Rev. Mod. Phys.* **90**, 025001 (2018), arXiv:1706.06223 [hep-lat].
[5] M. Mai, M. Döring, and A. Rusetsky, *Eur. Phys. J. ST* **230**, 1623 (2021), arXiv:2103.00577 [hep-lat].
[6] J. Bulava *et al.*, in *Snowmass 2021* (2022) arXiv:2203.03230 [hep-lat].
[7] M. Mai, U.-G. Meißner, and C. Urbach, *Phys. Rept.* **1001**, 1 (2023), arXiv:2206.01477 [hep-ph].
[8] T. Yamazaki *et al.* (CP-PACS), *Phys. Rev. D* **70**, 074513 (2004), arXiv:hep-lat/0402025.
[9] S. R. Beane, T. C. Luu, K. Orginos, A. Parreno, M. J. Savage, A. Torok, and A. Walker-Loud, *Phys. Rev. D* **77**, 014505 (2008), arXiv:0706.3026 [hep-lat].
[10] S. R. Beane, E. Chang, W. Detmold, H. W. Lin, T. C. Luu, K. Orginos, A. Parreno, M. J. Savage, A. Torok, and A. Walker-Loud (NPLQCD), *Phys. Rev. D* **85**, 034505 (2012), arXiv:1107.5023 [hep-lat].
[11] J. J. Dudek, R. G. Edwards, and C. E. Thomas, *Phys. Rev. D* **86**, 034031 (2012), arXiv:1203.6041 [hep-ph].
[12] Z. Fu, *Phys. Rev. D* **87**, 074501 (2013), arXiv:1303.0517 [hep-lat].
[13] J. Bulava, B. Fahy, B. Hörz, K. J. Juge, C. Morningstar, and C. H. Wong, *Nucl. Phys. B* **910**, 842 (2016), arXiv:1604.05593 [hep-lat].
[14] J.-J. Wu, W. Kamleh, D. B. Leinweber, Y. Li, G. Schierholz, R. D. Young, and J. M. Zanotti (CSSM-QCDSF), *Phys. Rev. D* **105**, 074506 (2022), arXiv:2109.01557 [hep-lat].
[15] K. Sasaki, N. Ishizuka, M. Oka, and T. Yamazaki (PACS-CS), *Phys. Rev. D* **89**, 054502 (2014), [Erratum: *Phys.Rev.D* 105, 019901 (2022)], arXiv:1311.7226 [hep-lat].
[16] T. D. Blanton, A. D. Hanlon, B. Hörz, C. Morningstar, F. Romero-López, and S. R. Sharpe, *JHEP* **10**, 023 (2021), arXiv:2106.05590 [hep-lat].
[17] S. R. Beane, T. C. Luu, K. Orginos, A. Parreno, M. J. Savage, A. Torok, and A. Walker-Loud (NPLQCD), *Phys. Rev. D* **77**, 094507 (2008), arXiv:0709.1169 [hep-lat].
[18] C. Helmes, C. Jost, B. Knippschild, B. Kostrzewa, L. Liu, C. Urbach, and M. Werner, *Phys. Rev. D* **96**, 034510 (2017), arXiv:1703.04737 [hep-lat].

- [19] R. Aaij *et al.* (LHCb), *Nature Phys.* **18**, 751 (2022), arXiv:2109.01038 [hep-ex].
- [20] R. Aaij *et al.* (LHCb), *Nature Commun.* **13**, 3351 (2022), arXiv:2109.01056 [hep-ex].
- [21] M.-J. Yan and M. P. Valderrama, *Phys. Rev. D* **105**, 014007 (2022), arXiv:2108.04785 [hep-ph].
- [22] S. Fleming, R. Hodges, and T. Mehen, *Phys. Rev. D* **104**, 116010 (2021), arXiv:2109.02188 [hep-ph].
- [23] L. Dai, S. Fleming, R. Hodges, and T. Mehen, *Phys. Rev. D* **107**, 076001 (2023), arXiv:2301.11950 [hep-ph].
- [24] F.-K. Guo, C. Hidalgo-Duque, J. Nieves, A. Ozpineci, and M. P. Valderrama, *Eur. Phys. J. C* **74**, 2885 (2014), arXiv:1404.1776 [hep-ph].
- [25] L. Dai, F.-K. Guo, and T. Mehen, *Phys. Rev. D* **101**, 054024 (2020), arXiv:1912.04317 [hep-ph].
- [26] M.-Z. Liu, T.-W. Wu, M. Pavon Valderrama, J.-J. Xie, and L.-S. Geng, *Phys. Rev. D* **99**, 094018 (2019), arXiv:1902.03044 [hep-ph].
- [27] A. Martínez Torres, K. P. Khemchandani, and L.-S. Geng, *Phys. Rev. D* **99**, 076017 (2019), arXiv:1809.01059 [hep-ph].
- [28] T.-W. Wu, M.-Z. Liu, L.-S. Geng, E. Hiyama, and M. P. Valderrama, *Phys. Rev. D* **100**, 034029 (2019), arXiv:1906.11995 [hep-ph].
- [29] Y. Huang, M.-Z. Liu, Y.-W. Pan, L.-S. Geng, A. Martínez Torres, and K. P. Khemchandani, *Phys. Rev. D* **101**, 014022 (2020), arXiv:1909.09021 [hep-ph].
- [30] Y.-W. Pan, J.-X. Lu, E. Hiyama, L.-S. Geng, and A. Hosaka, (2025), arXiv:2502.00438 [nucl-th].
- [31] J.-Y. Pang, J.-J. Wu, and L.-S. Geng, *Phys. Rev. D* **102**, 114515 (2020), arXiv:2008.13014 [hep-lat].
- [32] Q.-C. Xiao, J.-Y. Pang, and J.-J. Wu, *Phys. Rev. D* **110**, 094517 (2024), arXiv:2408.16590 [hep-lat].
- [33] Y. Li *et al.* (Belle), *Phys. Rev. D* **102**, 112001 (2020), arXiv:2008.13341 [hep-ex].
- [34] M. Padmanath and S. Prelovsek, *Phys. Rev. Lett.* **129**, 032002 (2022), arXiv:2202.10110 [hep-lat].
- [35] S. Chen, C. Shi, Y. Chen, M. Gong, Z. Liu, W. Sun, and R. Zhang, *Phys. Lett. B* **833**, 137391 (2022), arXiv:2206.06185 [hep-lat].
- [36] Y. Lyu, S. Aoki, T. Doi, T. Hatsuda, Y. Ikeda, and J. Meng, *Phys. Rev. Lett.* **131**, 161901 (2023), arXiv:2302.04505 [hep-lat].
- [37] T. Whyte, D. J. Wilson, and C. E. Thomas, (2024), arXiv:2405.15741 [hep-lat].
- [38] S. Collins, A. Nefediev, M. Padmanath, and S. Prelovsek, *Phys. Rev. D* **109**, 094509 (2024), arXiv:2402.14715 [hep-lat].
- [39] M. Abolnikov, V. Baru, E. Epelbaum, A. A. Filin, C. Hanhart, and L. Meng, *Phys. Lett. B* **860**, 139188 (2024), arXiv:2407.04649 [hep-ph].
- [40] M.-L. Du, A. Filin, V. Baru, X.-K. Dong, E. Epelbaum, F.-K. Guo, C. Hanhart, A. Nefediev, J. Nieves, and Q. Wang, *Phys. Rev. Lett.* **131**, 131903 (2023), arXiv:2303.09441 [hep-ph].
- [41] L. Meng, V. Baru, E. Epelbaum, A. A. Filin, and A. M. Gasparyan, *Phys. Rev. D* **109**, L071506 (2024), arXiv:2312.01930 [hep-lat].
- [42] A. B. a. Raposo and M. T. Hansen, *JHEP* **08**, 075 (2024), arXiv:2311.18793 [hep-lat].
- [43] R. Bubna, H.-W. Hammer, F. Müller, J.-Y. Pang, A. Rusetsky, and J.-J. Wu, *JHEP* **05**, 168 (2024),

- arXiv:2402.12985 [hep-lat].
- [44] M. T. Hansen, F. Romero-López, and S. R. Sharpe, *JHEP* **06**, 051 (2024), arXiv:2401.06609 [hep-lat].
- [45] M.-L. Du, F.-K. Guo, and B. Wu, (2024), 10.48550/arXiv.2408.09375, arXiv:2408.09375 [hep-ph].
- [46] Z.-C. Hu *et al.* (CLQCD), *Phys. Rev. D* **109**, 054507 (2024), arXiv:2310.00814 [hep-lat].
- [47] Q.-A. Zhang *et al.*, *Chin. Phys. C* **46**, 011002 (2022), arXiv:2103.07064 [hep-lat].
- [48] H. Xing, J. Liang, L. Liu, P. Sun, and Y.-B. Yang, (2022), arXiv:2210.08555 [hep-lat].
- [49] H. Liu, J. He, L. Liu, P. Sun, W. Wang, Y.-B. Yang, and Q.-A. Zhang, *Sci. China Phys. Mech. Astron.* **67**, 211011 (2024), arXiv:2207.00183 [hep-lat].
- [50] H. Liu, L. Liu, P. Sun, W. Sun, J.-X. Tan, W. Wang, Y.-B. Yang, and Q.-A. Zhang, *Phys. Lett. B* **841**, 137941 (2023), arXiv:2303.17865 [hep-lat].
- [51] H. Yan, C. Liu, L. Liu, Y. Meng, and H. Xing, (2024), arXiv:2404.13479 [hep-lat].
- [52] H.-Y. Du *et al.*, (2024), arXiv:2408.03548 [hep-lat].
- [53] Y. Meng, J.-L. Dang, C. Liu, Z. Liu, T. Shen, H. Yan, and K.-L. Zhang, *Phys. Rev. D* **109**, 074511 (2024), arXiv:2401.13475 [hep-lat].
- [54] M. Peardon, J. Bulava, J. Foley, C. Morningstar, J. Dudek, R. G. Edwards, B. Joó, H.-W. Lin, D. G. Richards, and K. J. Juge (Hadron Spectrum), *Phys. Rev. D* **80**, 054506 (2009), arXiv:0905.2160 [hep-lat].
- [55] M. Lüscher and U. Wolff, *Nucl. Phys. B* **339**, 222 (1990).
- [56] M. Göckeler, R. Horsley, M. Lage, U.-G. Meißner, P. E. L. Rakow, A. Rusetsky, G. Schierholz, and J. M. Zanotti, *Phys. Rev. D* **86**, 094513 (2012), arXiv:1206.4141 [hep-lat].
- [57] X.-K. Dong, F.-K. Guo, and B.-S. Zou, *Commun. Theor. Phys.* **73**, 125201 (2021), arXiv:2108.02673 [hep-ph].
- [58] L. Meng, E. Ortiz-Pacheco, V. Baru, E. Epelbaum, M. Padmanath, and S. Prelovsek, (2024), arXiv:2411.06266 [hep-lat].
- [59] R. G. Edwards and B. Joó (SciDAC, LHPC, UKQCD), *Nucl. Phys. B Proc. Suppl.* **140**, 832 (2005), arXiv:hep-lat/0409003.
- [60] M. A. Clark, R. Babich, K. Barros, R. C. Brower, and C. Rebbi (QUDA), *Comput. Phys. Commun.* **181**, 1517 (2010), arXiv:0911.3191 [hep-lat].
- [61] R. Babich, M. A. Clark, B. Joó, G. Shi, R. C. Brower, and S. Gottlieb (QUDA), in *International Conference for High Performance Computing, Networking, Storage and Analysis* (2011) arXiv:1109.2935 [hep-lat].
- [62] M. A. Clark, B. Joó, A. Strelchenko, M. Cheng, A. Gambhir, and R. C. Brower (QUDA), in *International Conference for High Performance Computing, Networking, Storage and Analysis* (2016) arXiv:1612.07873 [hep-lat].
- [63] M. Döring, U.-G. Meißner, E. Oset, and A. Rusetsky, *Eur. Phys. J. A* **47**, 139 (2011), arXiv:1107.3988 [hep-lat].
- [64] M. Döring, U.-G. Meißner, E. Oset, and A. Rusetsky, *Eur. Phys. J. A* **48**, 114 (2012), arXiv:1205.4838

[hep-lat].

- [65] C. H. Kim, C. T. Sachrajda, and S. R. Sharpe, *Nucl. Phys. B* **727**, 218 (2005), arXiv:hep-lat/0507006.
- [66] Y. Li, J.-J. Wu, T. S. H. Lee, and R. D. Young, *JHEP* **08**, 178 (2024), arXiv:2404.16702 [hep-lat].